Geomechanics and Engineering, *Vol. 28, No. 5 (2022) 493-503*
https://doi.org/10.12989/gae.2022.28.5.493

Drained cylindrical cavity expansion in K_0-consolidated anisotropic soils under biaxial in-situ stresses

Xiaobing Cao[1], Junran Zhang*[2] and De'an Sun**[3]

[1]*Department of Geotechnical Engineering, Tongji University, Shanghai 200092, China*
[2]*Henan Province Key Laboratory of Geomechanics and Structural Engineering, North China University of Water Resources and Electric Power, Zhengzhou, Henan 450046, China*
[3]*Department of Civil Engineering, Shanghai University, Shanghai 200444, China*

(Received September 3, 2021, Revised January 20, 2022, Accepted January 22, 2022)

Abstract. Cavity expansion is a classical problem in the field of solid mechanics with a wide range of applications in geotechnical and petroleum engineering. A drained solution is developed for cylindrical cavity expansion in anisotropic soils under biaxial in-situ stresses using a K0-based anisotropic modified Cam-clay model (K0-AMCC). The problem is formulated by solving differential equations using an auxiliary variable, which provides analytical expressions for the volume and four stress components of the soil around the cylindrical cavity. The solution is validated by comparisons with existing well-developed solutions. The results show that the present solution well captures the cavity expansion responses in anisotropic soils under biaxial in-situ stresses, and removes limiting assumptions that the cylindrical cavity expands under uniform in-situ stress in isotropic soils. The elastic-plastic boundary of the expanding cylindrical cavity in K0-consolidated anisotropic soils under biaxial in-situ stresses is a circle rather than an ellipse in isotropic soils, and the mathematical proof is provided in detail.

Keywords: anisotropic; biaxial in-situ stresses; circle; drained; elastic-plastic boundary; K_0-consolidated

1. Introduction

Since cavity expansion theory was initially proposed by Lamé (1852), extensive research to improve the solutions for cavity expansion because of its successful and increasingly promising applications in both geotechnical, petroleum and tunnel engineering (e.g., Carter *et al*. 1986, Collins and Yu 1996, Salgado *et al.* 1997, Yu 2000, Chang *et al.* 2001, Cao *et al*. 2002, Russell and Khalili 2002, Salgado and Prezzi 2007, Vrakas and Anagnostou 2015, Gong *et al*. 2017, Li and Gong 2019, Tan *et al*. 2022, Zhou *et al.* 2022). In recent years, significant progress has further improved the cavity expansion theory by applying sophisticated constitutive models to more realistic simulations of soil behavior. For example, Yang and Zou (2011) proposed expansion solutions for cylindrical and spherical cavities using a non-linear failure criterion that considers the effects of soil dilatancy. Chen and Abousleiman (2013) developed drained solutions for the expansion of cylindrical cavity by incorporating the Modified Cam-clay (MCC) model and rigorous definitions of mean and deviator stresses. Zhou *et al*. (2018) used an advanced constitutive model for thermoplasticity to build a similar framework that explores the cavity expansion in thermoplastic soils. Although several types of constitutive soil models have been used to simulate soil behavior or describe various soil properties, the significantly anisotropic properties of soils, which are the intrinsic properties for most natural soils because they were consolidated under the K_0 condition, have been largely ignored in previous studies.

A few solutions of cavity expansion in anisotropic soils are presently available (e.g., Sivasithamparam and Castro, 2020, Li *et al*. 2019, Liu and Chen 2019, Wang *et al*. 2021, Chen *et al*. 2021). These solutions are implemented using various advanced soil constitutive models to consider the initial anisotropy, stress induced anisotropy, and even fabric anisotropy. However, in their theoretical frameworks, the cylindrical cavity expands under uniform stress whereas realistic in-situ stresses under a variety of conditions are biaxial, particularly for horizontal wellbore drilling, underground structures at a relatively shallow burial depth, and tunnel excavating.

To remove limitations from the available drained solutions for the expansion of cylindrical cavity involved in the assumption that a cylindrical cavity can only expand under uniform in-situ stress in isotropic soils, a theoretical framework is here proposed to simulate the drained expansion of cylindrical cavity in K_0-consolidated anisotropic soils under biaxial stresses. The solution is divided into three parts: 1) K_0-based anisotropic MCC model: the K_0-AMCC model is used to simulate soil response during the cavity expansion that considers the effect of initial stress anisotropy. 2) Elasto-plastic analysis:

The variations in specific volume and four stresses around the cylindrical cavity during the expansion are explored in detail to identify differences with those around the cylindrical cavity in soils under uniform in-situ stress. 3)

*Corresponding author, Professor
E-mail: zhangjunran@ncwu.edu.cn
**Corresponding author, Professor
E-mail: sundean@shu.edu.cn

ISSN: 2005-307X (Print), 2092-6219 (Online)

Validation and Discussion: The solution is validated by comparisons with a solution obtained under conditions of biaxial in-situ stresses in isotropic soil. The proposed solution enriches the cavity expansion theory and provides a more realistic tool for applications in geotechnical and petroleum engineering.

2. In-situ stresses and equilibrium equation

The underlying assumptions involved in developing the present drained solution for the expansion of cylindrical cavity in K_0-consolidated anisotropic soil under in-situ biaxial stresses are listed below.

(1) The compression stress and clockwise shear stress are conventionally positive.

(2) The problem of the cylindrical cavity expansion belongs to a plane strain problem. Because of the drained condition, no excess pore water pressures are generated during the cavity expansion and all stresses mentioned here are effective stresses (e.g., an apostrophe is not used to denote effective stresses).

(3) The soil is homogeneous. Small deformation theory is adopted to describe soil behavior in the elastic region, whereas soil behavior after yielding can be appropriately simulated by the K_0-AMCC model and large deformation theory.

Fig. 1 presents a schematic diagram of the cylindrical cavity expansion under biaxial in-situ stresses. The cylindrical cavity is with the initial radius, a_0, and initial internal expansion stress, σ_0. During the expansion, the cylindrical cavity is subjected to in-plane biaxial in-situ stresses, σ_{x0} and σ_{y0}, and out-of-plane stress, σ_{z0}. Owing to the biaxial in-situ stresses (i.e. $\sigma_{x0} \neq \sigma_{y0}$), the shear stress is initially induced in the soil around the cavity. This is one of the most prominent features that differs from conventional cylindrical cavity expansion under uniform in-situ stress. The in-situ stresses are perpendicular to one another along the x- and y-axes, whereas polar coordinates are less labor intensive in the formulation of cavity expansion problems. A stress transformation is therefore given between the two coordinate systems

$$\sigma_{r0}=\sigma_{x0}\cos^2\theta+\sigma_{y0}\sin^2\theta \tag{1}$$

$$\sigma_{\theta 0}=\sigma_{x0}\sin^2\theta+\sigma_{y0}\cos^2\theta \tag{2}$$

$$\sigma_{z0}=\sigma_{z0} \tag{3}$$

$$\tau_{r\theta 0}=\left(\sigma_{x0}-\sigma_{y0}\right)\sin\theta\cos\theta \tag{4}$$

where σ_{r0}, $\sigma_{\theta 0}$, and $\tau_{r\theta 0}$ are the initial radial, circumferential, and shear stresses, respectively.

As the cylindrical cavity radius increases from its initial to present value, a, a corresponding radial pressure change occurs from its initial to current values, σ_a. Because of the symmetry of the internal uniform stress and initial circular cavity shape in the Cartesian coordinate system, the shear stress is not present on the cavity wall. Hence, the

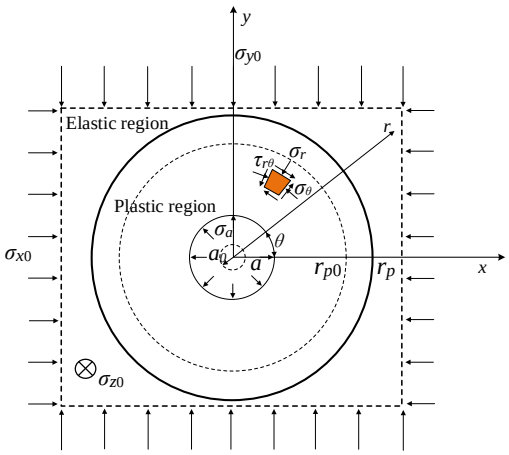

Fig. 1 Schematic diagram of cylindrical cavity expansion under biaxial in-situ stresses

cylindrical cavity expands uniformly and maintains its initial circular shape during the entire expansion process. Correspondingly, the material particle changes from its initial position (r_0, θ) to the present position (r, θ) without changing the circumferential coordinate and only undergoing radial displacement, u_r, which is equal to $r - r_0$. The soil around the cavity wall yields with increasing the radial uniform stress, which results in an annular plastic region with a range from a to the elastic-plastic (E-P) boundary, r_p. The shape of the E-P boundary is a circle during the expansion, which is critically different from the elliptic shape of the E-P boundary in the cylindrical solution under biaxial in-situ stresses but in isotropic soils (Zhuang and Yu 2019, Yang *et al*. 2020). The soil outside of the E-P boundary performs elastically regardless of increasing the internal expansion pressure. The E-P boundary is a circle (Fig. 1), and the mathematical proof will be provided in Section 7.4.

In the elastic or plastic zone, the material particle at radial position (r, θ) must satisfy the differential equation of the equilibrium during the entire expansion process, which can be expressed as

$$\frac{\partial\sigma_r}{\partial r}+\frac{1}{r}\frac{\partial\tau_{r\theta}}{\partial\theta}+\frac{\sigma_r-\sigma_\theta}{r}=0 \tag{5}$$

where σ_r, σ_θ, and $\tau_{r\theta}$ are the initial radial, circumferential, and shear stresses, respectively.

3. Elastic analysis

The stress-strain relationship of material particles in the elastic region during the cavity expansion can be determined based on the generalized Hooke's law as

$$\begin{bmatrix} d\varepsilon_r^e \\ d\varepsilon_\theta^e \\ d\varepsilon_z^e \\ d\varepsilon_{r\theta}^e \end{bmatrix}=\begin{bmatrix} \frac{1}{E} & -\frac{\mu}{E} & -\frac{\mu}{E} & 0 \\ -\frac{\mu}{E} & \frac{1}{E} & -\frac{\mu}{E} & 0 \\ -\frac{\mu}{E} & -\frac{\mu}{E} & \frac{1}{E} & 0 \\ 0 & 0 & 0 & \frac{1+\mu}{E} \end{bmatrix}\begin{bmatrix} d\sigma_r' \\ d\sigma_\theta' \\ d\sigma_z' \\ d\tau_{r\theta} \end{bmatrix} \tag{6}$$

where $d\varepsilon_r$, $d\varepsilon_\theta$, $d\varepsilon_z$, and $d\varepsilon_{r\theta}$ are the radial, circumferential, vertical, and shear strain increments, respectively; $d\sigma_r$, $d\sigma_\theta$, $d\sigma_z$, and $d\tau_{r\theta}$ are the radial, circumferential, vertical, and shear stress increments, respectively, and μ denotes Poisson's ratio, E denotes Young's modulus, and the calculation expression is $E = 2G(1 + \mu)$. In the MCC model, the elastic shear modulus, G, is given as (Wood 1990)

$$G = \frac{3(1-2\mu)vp}{2(1+\mu)\kappa} \tag{7}$$

where $v = 1 + e$ denotes specific volume and e is the void ratio. In the v-ln p plane, the slopes of the reloading lines is denoted by κ, and the mean stress is denoted by p. Because an infinitesimal stress increment makes no difference in the mean and deviator stresses, parameters E, G, and v are considered constant, and the values equal to the initial values in the elastic analysis.

The solutions for the stresses and radial displacements in the elastic region can be derived based on small strain deformation theory by combining Eqs. (1)- (5) as follows (Timoshenko and Goodier 1970)

$$\begin{aligned}\sigma_r &= \sigma_{r0} + \delta\sigma_a\left(\frac{r_p}{r}\right)^2 = \sigma_{x0}\cos^2\theta \\ &+ \sigma_{y0}\sin^2\theta + \delta\sigma_a\left(\frac{r_p}{r}\right)^2\end{aligned} \tag{8}$$

$$\begin{aligned}\sigma_\theta &= \sigma_{\theta0} + \delta\sigma_a\left(\frac{r_p}{r}\right)^2 = \sigma_{x0}\sin^2\theta \\ &+ \sigma_{y0}\cos^2\theta - \delta\sigma_a\left(\frac{r_p}{r}\right)^2\end{aligned} \tag{9}$$

$$\sigma_z = \sigma_{z0} \tag{10}$$

$$\tau_{r\theta} = \tau_{r\theta0} = \left(\sigma_{x0} - \sigma_{y0}\right)\sin\theta\cos\theta \tag{11}$$

$$u_r = \frac{\delta\sigma_a}{2G_0}\frac{r_p^2}{r} \tag{12}$$

where $\delta\sigma_a$ denotes the stress increment at the cavity wall.

4. K_0-based anisotropic MCC model

Roscoe and Burland (1968) proposed a classical modified Cam-clay (MCC) model, and the MCC model has many advantages. However, the MCC model cannot simulate the anisotropic behavior of natural soils during the cylindrical cavity expansion. Sekiguchi and Ohta (1977) proposed an elastoplastic model for the initially anisotropic clays, which remains limited in its description of anisotropic soil behavior. The K_0-AMCC model was presented by Sun *et al*. (2004), which accounts for the initial stress anisotropy, and is used to simulate the problem of cavity expansion. The yield function in the K_0-AMCC model is expressed as

$$f = 1 + \left(\frac{\eta^*}{M^*}\right)^2 - \frac{p_c}{p} = 0 \tag{13}$$

where p_c is the hardening parameter for the model and η^* and M^* are the stress ratio and stress ratio at the critical state, respectively, and are expressed as

$$\eta^* = \sqrt{\frac{3}{2}(\eta_{iij} - \eta_{ij0})(\eta_{iij} - \eta_{ij0})} \tag{14}$$

$$M^* = \sqrt{M^2 - \eta_0^2} \tag{15}$$

where

$$\eta_{ij} = \frac{\sigma_{ij} - p\delta_{ij}}{p} \tag{16}$$

$$\eta_{ij0} = \frac{\sigma_{ij0} - p_0\delta_{ij}}{p_0} \tag{17}$$

$$\eta_0 = \left|\frac{3(1-K_0)}{2K_0+1}\right| \tag{18}$$

$$M = \frac{6\sin\varphi}{3-\sin\varphi} \tag{19}$$

where σ_{ij} denotes the stress tensor, Kronecker's delta is denoted by δ_{ij}, p_0 is the initial mean stress, the slope of the critical state line is denoted by M, the internal friction angle is denoted by φ, and η_0 is relative stress ratio at the initial state.

5. Elasto-plastic analysis

Soil behavior in the plastic region is described by the K_o-MCC model, which assumes that the soil is a type of volumetric hardening material and obeys the associated flow rule. The plastic strain increments can be calculated as

$$d\varepsilon_{ij}^p = \Lambda\frac{\partial f}{\partial\sigma_{ij}} \tag{20}$$

where Λ denotes a plastic multiplier expressed as

$$\Lambda = \frac{\frac{\partial f}{\partial\eta^*}d\eta^* + \frac{\partial f}{\partial p}dp}{\frac{\upsilon_0}{\lambda-\kappa}\frac{\partial f}{\partial p_c}p_c\left(\frac{\partial f}{\partial\sigma_r} + \frac{\partial f}{\partial\sigma_\theta} + \frac{\partial f}{\partial\sigma_z}\right)} \tag{21}$$

where v_0 denotes the initial value of the specific volume. In the e-ln p plane, the slopes of the two lines are denoted by λ and κ for the initial isotropic loading and reloading condition, respectively. The concrete derivative expressions are given as follows

$$\frac{\partial f}{\partial\eta^*} = \frac{2\eta^*}{M^{*2}},\quad \frac{\partial f}{\partial p} = \frac{p_c}{p^2},\quad \frac{\partial f}{\partial p_c} = -\frac{1}{p} \tag{22}$$

$$d\eta^* = \frac{1}{2\eta^* p}[3(\eta_{ij} - \eta_{ij0}) + \eta_{mn}(\eta_{mn} - \eta_{mn0})\delta_{ij}]\sigma_{ij} \tag{23}$$

$$dp = \frac{\delta_{ij}}{3}\sigma_{ij} \tag{24}$$

$$\frac{\partial f}{\partial \sigma_i} = \frac{M^{*2}+\eta^{*2}}{3pM^{*2}} + \frac{1}{pM^{*2}}[3(\eta_{ij}-\eta_{ij0}) + \eta_{mn}(\eta_{mn}-\eta_{mn0})], (i=j=r,\theta,z) \tag{25}$$

The rates of plastic strain for a material particle around the cylindrical cavity can be expressed by combining Eqs. (20) and (21) as

$$d\varepsilon_{ij}^{p} = \frac{\lambda-\kappa}{1+e}\frac{\left(M^{*2}+\eta^{*2}\right)}{p\left(M^{2}-\eta^{2}\right)} \left[\frac{\delta_{ij}}{3}+\frac{3\left(\eta_{ij}-\eta_{ij0}\right)-\eta_{mn}\left(\eta_{mn}-\eta_{mn0}\right)\delta_{ij}}{\left(M^{*2}+\eta^{*2}\right)}\right] \left[\frac{\delta_{ij}}{3}+\frac{3\left(\eta_{ij}-\eta_{ij0}\right)-\eta_{mn}\left(\eta_{mn}-\eta_{mn0}\right)\delta_{ij}}{\left(M^{*2}+\eta^{*2}\right)}\right] d\sigma_{ij} \tag{26}$$

The plastic stress-strain relationship can be calculated and is shown here in matrix form as

$$\begin{bmatrix} d\varepsilon_r^p \\ d\varepsilon_\theta^p \\ d\varepsilon_z^p \\ d\varepsilon_{r\theta}^p \end{bmatrix} = A \begin{bmatrix} A_r^2 & A_rA_\theta & A_rA_z & A_rA_{r\theta} \\ A_\theta A_r & A_\theta^2 & A_\theta A_z & A_\theta A_{r\theta} \\ A_zA_r & A_zA_\theta & A_z^2 & A_zA_{r\theta} \\ A_{r\theta}A_r & A_{r\theta}A_\theta & A_{r\theta}A_z & A_{r\theta}^2 \end{bmatrix} \begin{bmatrix} d\sigma_r \\ d\sigma_\theta \\ d\sigma_z \\ d\tau_{r\theta} \end{bmatrix} \tag{27}$$

where A, A_r, A_θ, A_z, and $A_{r\theta}$ are presented in Appendix.

Using the solutions of the elastic and plastic stress-strain relationships (Eqs. (6), (27)), the elastoplastic constitutive equation can be obtained as

$$\begin{bmatrix} d\varepsilon_r^p \\ d\varepsilon_\theta^p \\ d\varepsilon_z^p \\ d\varepsilon_{r\theta}^p \end{bmatrix} = \begin{bmatrix} \frac{1}{E}+AA_r^2 & -\frac{\mu}{E}+AA_rA_\theta & -\frac{\mu}{E}+AA_rA_z & AA_rA_{r\theta} \\ -\frac{\mu}{E}+AA_\theta A_r & \frac{1}{E}+AA_\theta^2 & -\frac{\mu}{E}+AA_\theta A_z & AA_\theta A_{r\theta} \\ -\frac{\mu}{E}+AA_zA_r & -\frac{\mu}{E}+AA_zA_\theta & \frac{1}{E}+AA_z^2 & AA_zA_{r\theta} \\ AA_{r\theta}A_r & AA_{r\theta}A_\theta & AA_{r\theta}A_z & \frac{1+\mu}{E}+AA_{r\theta}^2 \end{bmatrix} \begin{bmatrix} d\sigma_r \\ d\sigma_\theta \\ d\sigma_z \\ d\tau_{r\theta} \end{bmatrix} \tag{28}$$

Using the matrix inversion calculation, the elastoplastic constitutive equation can be further expressed as

$$\begin{bmatrix} d\sigma_r \\ d\sigma_\theta \\ d\sigma_z \\ d\tau_{r\theta} \end{bmatrix} = \frac{1}{B}\begin{bmatrix} B_{11} & B_{12} & B_{13} & B_{14} \\ B_{21} & B_{22} & B_{23} & B_{24} \\ B_{31} & B_{32} & B_{33} & B_{34} \\ B_{41} & B_{42} & B_{43} & B_{44} \end{bmatrix} \begin{bmatrix} d\varepsilon_r^p \\ d\varepsilon_\theta^p \\ d\varepsilon_z^p \\ d\varepsilon_{r\theta}^p \end{bmatrix} \tag{29}$$

where B and B_{ij} are presented in Appendix.

For the cylindrical cavity expansion, $d\varepsilon_z = 0$ under the plane strain conditions. Thus, the relationship of incremental volumetric strain can be expressed as

$$d\varepsilon_v = d\varepsilon_r + d\varepsilon_\theta \tag{30}$$

where

$$d\varepsilon_v = -\frac{dv}{v} \tag{31}$$

where the specific volume is denoted by $v = 1 + e$. Substituting Eqs. (30) and (31) into Eq. (29) yields

$$d\sigma_r = \frac{1}{B}[B_{11}d\varepsilon_v + (B_{12}-B_{11})d\varepsilon_\theta] \tag{32}$$

$$d\sigma_\theta = \frac{1}{B}[B_{21}d\varepsilon_v + (B_{22}-B_{21})d\varepsilon_\theta] \tag{33}$$

$$d\sigma_z = \frac{1}{B}[B_{31}d\varepsilon_v + (B_{32}-B_{31})d\varepsilon_\theta] \tag{34}$$

$$d\tau_{r\theta} = \frac{1}{B}[B_{41}d\varepsilon_v + (B_{42}-B_{41})d\varepsilon_\theta] \tag{35}$$

In the plastic zone, the increment of tangential strain can be considered the large deformation and is expressed in logarithmic form as

$$d\varepsilon_\theta = -\frac{dr}{r} \tag{36}$$

where dr represents the infinitesimal radial increment.

The specific volume changes during the cavity expansion under drained conditions (i.e., $dv = 1 + e \neq 0$) must be derived. The equations of the constitutive relationship have four unknown variables but there are only three equations, which makes it difficult to directly calculate the stress components. An auxiliary variable is imported to overcome this barrier, which is expressed as (Chen and Abousleiman 2013)

$$\xi = \frac{u_r}{r} = \frac{r-r_0}{r} \tag{37}$$

Under plane strain and drained conditions, the radial strain, ε_r, can be expressed as

$$\varepsilon_r = \varepsilon_v - \varepsilon_\theta = -\ln(\frac{v}{v_0}) + \ln(\frac{r}{r_0}) = \ln\frac{v_0}{v(1-\xi)} \tag{38}$$

The natural radial strain is derived and expressed as

$$\varepsilon_r = \varepsilon_v - \varepsilon_\theta = -\ln(\frac{dr}{dr_0}) = -\ln(1+\frac{du}{dr}\frac{dr}{dr_0}) = -\ln(1+\frac{du}{dr}e^{-\varepsilon_r}) \tag{39}$$

Combining Eqs. (38) and (39) gives

$$\frac{du_r}{dr} = 1 - \frac{v_0}{v(1-\xi)} \tag{40}$$

where v_0 is the initial value of the specific volume.

With the aid of the auxiliary variable, Eq. (5) can be rewritten as

$$\frac{d\sigma_r}{d\xi}\frac{d\xi}{dr} + \frac{1}{r}\frac{d\tau_{r\theta}}{d\theta} + \frac{\sigma_r-\sigma_\theta}{r} = 0 \tag{41}$$

Where

$$\frac{d\xi}{dr} = -\frac{\xi}{r} + \frac{1}{r}\frac{du_r}{dr} \tag{42}$$

Substituting Eqs. (36), (37) and (40) into Eqs. (32)- (35) gives

$$\frac{d\sigma_r}{d\xi} = -\frac{\sigma_r-\sigma_\theta+d\tau_{r\theta}/d\theta}{1-\xi-v_0/[v(1-\xi)]} \tag{43}$$

$$\frac{d\sigma_\theta}{d\xi} = -\frac{B_{21}}{B_{11}}\left\{\frac{B_{11}-B_{12}}{B(1-\xi)} + \frac{d\tau_{r\theta}/d\theta+\sigma_r-\sigma_\theta}{1-\xi-v_0/[v(1-\xi)]}\right\} - \frac{B_{22}-B_{21}}{B(1-\xi)} \tag{44}$$

$$\frac{d\sigma_z}{d\xi} = -\frac{B_{31}}{B_{11}}\left\{\frac{B_{11}-B_{12}}{B(1-\xi)} + \frac{d\tau_{r\theta}/d\theta+\sigma_r-\sigma_\theta}{1-\xi-v_0/[v(1-\xi)]}\right\} - \frac{B_{32}-B_{31}}{B(1-\xi)} \tag{45}$$

$$\frac{d\tau_{r\theta}}{d\xi}=-\frac{B_{41}}{B_{11}}\left\{\frac{B_{11}-B_{12}}{B(1-\xi)}+\frac{d\tau_{r\theta}/d\theta+\sigma_r-\sigma_\theta}{1-\xi-v_0/[v(1-\xi)]}\right\}-\frac{B_{42}-B_{41}}{B(1-\xi)} \quad (46)$$

$$\frac{dv}{d\xi}=-\frac{Bv}{B_{11}}\left\{\frac{B_{12}-B_{11}}{B(\xi-1)}+\frac{d\tau_{r\theta}/d\theta+(\sigma_r-\sigma_\theta)}{1-\xi-v_0/[v(1-\xi)]}\right\} \quad (47)$$

As long as the boundary conditions hold, a solution of the previous equations can be obtained. The boundary conditions will be presented for details in section 6. The relationship between r and ξ should be built to express the position r. Differentiating Eq. (37) for r gives

$$\frac{du_r}{dr}=\xi+r\frac{d\xi}{dr} \quad (48)$$

Combining Eqs. (40) and (48) yields

$$\xi+r\frac{d\xi}{dr}=1-\frac{v_0}{v(1-\xi)} \quad (49)$$

Integrating Eq. (49) yields

$$\frac{r}{a}=\exp\left(\int_{\xi_a}^{\xi}\frac{d\xi}{1-\xi-v_0/[v(1-\xi)]}\right) \quad (50)$$

6. Boundary conditions

The stresses at the E-P boundary for drained cylindrical cavity expansion can be expressed as (Yang *et al.* 2020)

$$\sigma_{rp}=\sigma_{r0}+\delta\sigma_a\left(\frac{r_p}{r}\right)^2=\sigma_{x0}\cos^2\theta+\sigma_{y0}\sin^2\theta+\delta\sigma_a \quad (51)$$

$$\sigma_{\theta p}=\sigma_{\theta 0}+\delta\sigma_a\left(\frac{r_p}{r}\right)^2=\sigma_{x0}\sin^2\theta+\sigma_{y0}\cos^2\theta-\delta\sigma_a \quad (52)$$

$$\sigma_{zp}=\sigma_{z0} \quad (53)$$

$$\tau_{r\theta p}=\tau_{r\theta 0}=(\sigma_{x0}-\sigma_{y0})\sin\theta\cos\theta \quad (54)$$

The stress state of soil particles at the E-P boundary is located on the yield surface. The relative stress ratio at the E-P boundary, η_p^*, is

$$\eta_p^*(\xi_p)=M^*\sqrt{OCR-1} \quad (55)$$

The specific formula is expanded as

$$\eta_p^*=\sqrt{\frac{3}{2}\left[\left(\frac{\sigma_{rp}}{p_p}-\frac{\sigma_{ro}}{p_o}\right)^2+\left(\frac{\sigma_{\theta p}}{p_p}-\frac{\sigma_{\theta o}}{p_o}\right)^2+\left(\frac{\sigma_{zp}}{p_p}-\frac{\sigma_{zo}}{p_o}\right)^2+2\left(\frac{\tau_{rzp}}{p_p}-\frac{\tau_{rzo}}{p_o}\right)^2\right]} \quad (56)$$

where

$$\delta\sigma_a=\frac{\sqrt{3}}{3}M^*p_0\sqrt{OCR-1} \quad (57)$$

The value of specific volume(v) atr the E-P boundary is equal to that in the elastic zone and it can be written as

$$v(\xi_p)=v_0 \quad (58)$$

where

$$\xi_p=\frac{u_r}{r}\Big|r=r_p \quad (59)$$

Based on the above boundary conditions, the stresses and volume around the cavity in anisotropic soils under drained conditions can be determined by solving the differential equations (Eqs. (43)-(47)).

Thus, A drained solution is developed for cylindrical cavity expansion in anisotropic soils under biaxial in-situ stresses using a K_0-based anisotropic modified Cam-clay model (K_0-AMCC).

7. Validation and discussion

The distribution of the four stresses and variation of specific volume around the cavity at different radial directions (θ) are discussed in detail in this section. The variation of position and shape of the E-P boundary is also explored to determine which factors have significant effects. To examine the validity of the proposed solution, the results obtained from the proposed analytical solution are compared with those from the solution by Yang *et al.* (2020). The parameters for soil properties and initial stresses used for the calculations are given in Table 1.

7.1 Stress distribution and variations of specific volume

To explore the stress distributions and variation of the specific volume at different θ, two different in-situ stresses along the x- and y-axes are adopted. Here, the non-isotropic case C in Table 1 is adopted (i.e., in-situ stress along the x-axis, σ_{x0} = 100 kPa, and σ_{y0} = 160 kPa). Figs. 2-6 show the distributions of radial, circumferential, vertical, and shear stresses and the variation of specific volume at the instant a/a_0 = 2 in five radial directions (θ = 0°, 30°, 45°, 60°, 90°). To further check the validity of the present solution, Figs. 2-6 also show the results from Yang *et al.* (2020) without considering soil anisotropy.

The radial distance of a material particle is normalized to the present radius, a. For the case where θ = 0° (Fig. 2), the shear stress $\tau_{r\theta}$ is found to always equal zero. This is because the soil element along this direction is under the axisymmetric condition and always in the principal stress

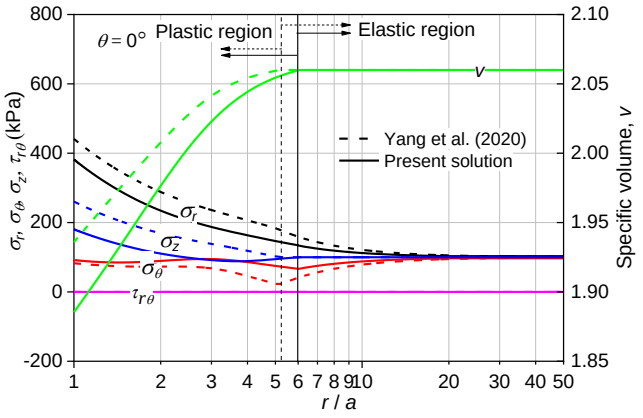

Fig. 2 Distributions of stresses and variation of specific volume for θ = 0°

Table 1 Parameters for validation and parametric study

Case	OCR	σ_{x0} (kPa)	σ_{y0} (kPa)	σ_{z0} (kPa)	p_0 (kPa)	q_0 (kPa)	υ_0	G_0 (kPa)
A	10	72	144	144	120	72	2.06	4302
B	3	90	135	135	120	90	2.06	4302
C	1.2	100	160	100	120	60	2.06	4302

$M = 1,\ \lambda = 0.15,\ \kappa = 0.03,\ \mu = 0.278,\ \upsilon_{cs} = 2.74$

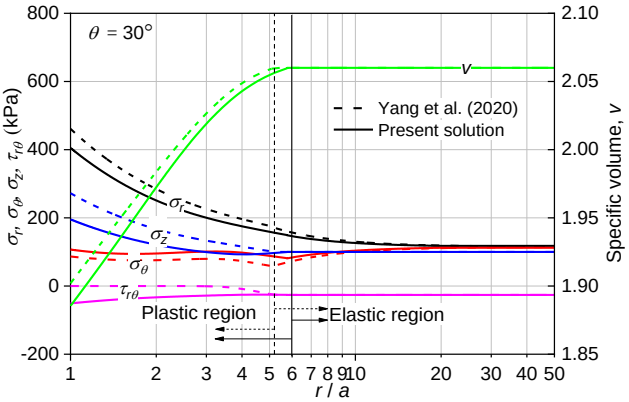

Fig. 3 Distributions of stresses and variation of specific volume for $\theta = 30°$

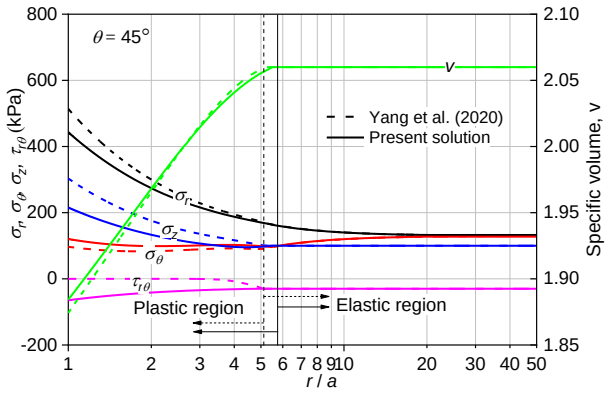

Fig. 4 Distributions of stresses and variation of specific volume for $\theta = 45°$

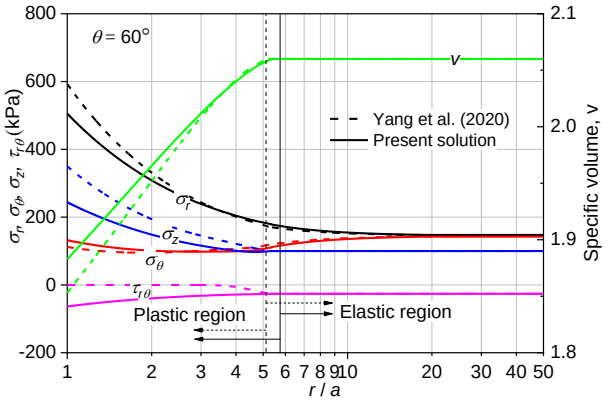

Fig. 5 Distributions of stresses and variation of specific volume for $\theta = 60°$

state regardless of the material particle's distance from the cylindrical cavity wall. For $\theta = 90°$ (Fig. 6), the shear stress,

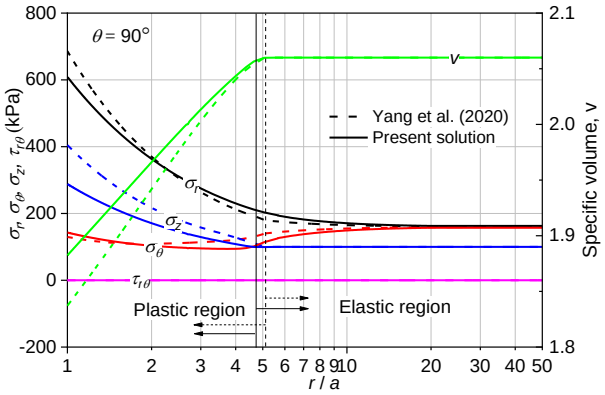

Fig. 6 Distributions of stresses and variation of specific volume for $\theta = 90°$

$\tau_{r\theta} = 0$, owing to the geometric symmetry. For cases where $\theta = 30°$ (Fig. 3), $\theta = 45°$ (Fig. 4), and $\theta = 60°$ (Fig. 5), $\tau_{r\theta}$ is not zero, which confirms that the cylindrical cavity maintains its initially anisotropic state. The $\tau_{r\theta}$ decreases with the increase in normalized radial distance (r/a) under the conditions of $r/a \leq 5$. As $r/a > 5$, the shear stress reaches a minimum and remains stable. Outside of the E-P boundary (i.e., in the elastic region), the shear stress remains constant and is equal to the minimum value. The $\tau_{r\theta}$ reaches a maximum when $\theta = 45°$. This differs from the results of Yang *et al.* (2020), where $\tau_{r\theta} = 0$ in the vicinity of cavity wall ($r/a \leq 3$), and because the normalized radial distance is greater than 3, the shear stress reaches a maximum.

Figs. 2-6 also show that both radial and vertical stresses in the plastic region decrease with increasing the normalized radial distance. However, after entering the elastic region, the radial stress continues to decrease to a certain value and then remains constant, whereas the vertical stress always remains constant. Compared with the results of Yang *et al.* (2020), the proposed solution underestimates the radial and vertical stresses.

When $\theta < 45°$, the circumferential stress initially decreases with increasing the normalized radial distance in the plastic region and then increases once the normalized radial distance exceeds the E-P boundary radius. In contrast, when $45° \leq \theta \leq 90°$, the circumferential stress initially decreases slightly and then increases in the plastic and elastic regions. Interestingly, all of the three normal stresses at the cavity wall increase with increasing θ, which may be attributed to the fact that stress along the y-axis is higher than along the x-axis. Compared with the results of Yang *et al.* (2020), the proposed solution overestimates the circumferential stress in the case of $\theta = 45°$. When $\theta > 45°$, the proposed solution first overestimates the circumferential

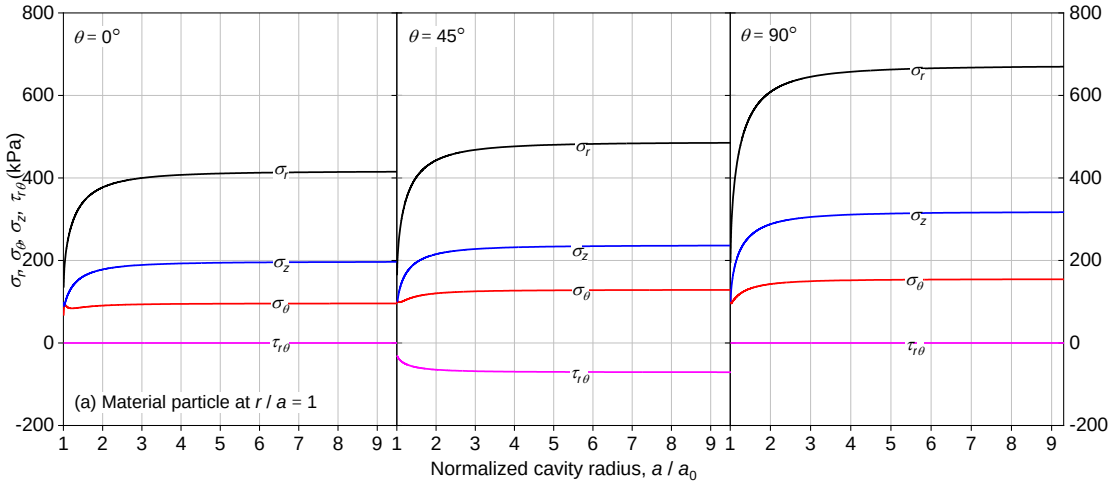

(a) $r/a = 1$

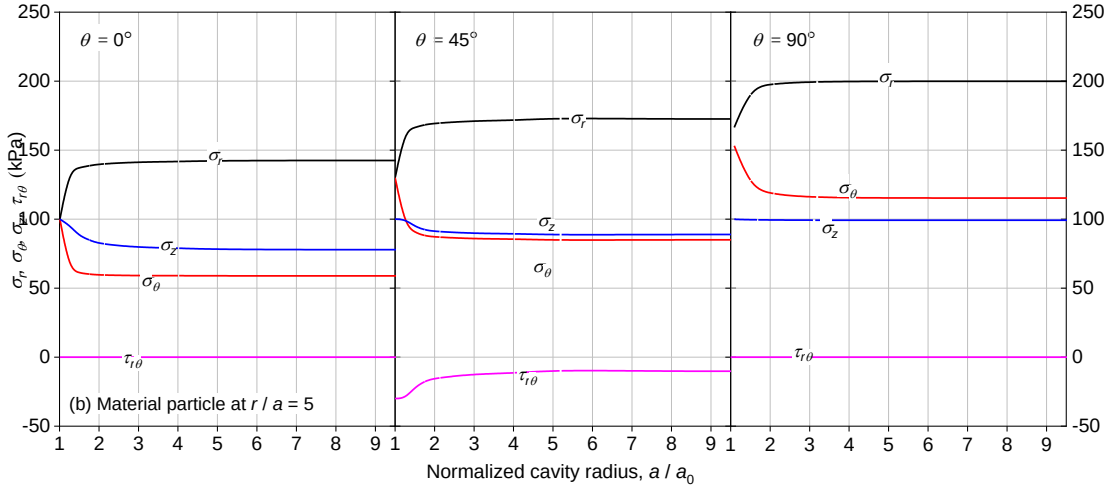

(b) $r/a = 5$

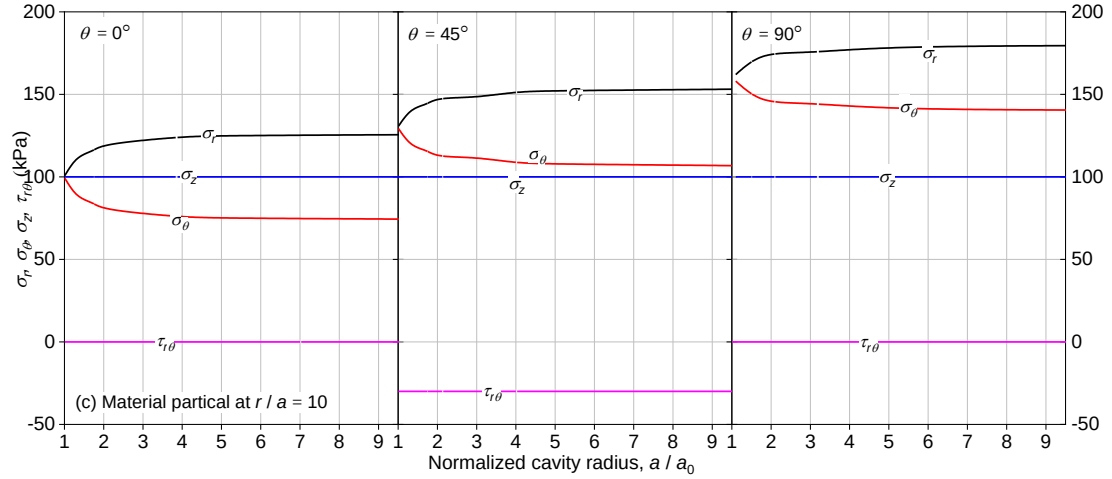

(c) $r/a = 10$

Fig. 7 Variation of stress components as a function of normalized cavity radius for different radial positions

stress in the plastic region and then underestimates the circumferential stress after the normalized radial distance exceeds the E-P boundary radius.

The specific volume increases with increasing the normalized radial distance in plastic region and then remains constant in the elastic region regardless of θ.

Compared with the results of Yang *et al*. (2020), the proposed solution overestimates the specific volume in the plastic region, and is consistent with the solution of Yang *et al.* (2020) and is equal to the initial value in the elastic region.

7.2 Expansion process

Fig. 7 presents the variations of stresses in material particles at positions r/a =1 (i.e., cavity wall), r/a = 5, and r/a =10 during the cavity expansion. Fig. 7(a) shows the relationship between the four stress components at the cavity wall and a/a_0. All of the stress components, except for the shear stress, change noticeably during the early cavity expansion stage. More specifically, both the radial stress, σ_r, and vertical stress, σ_z, increase, whereas the circumferential stress, σ_θ, initially decreases and then increases. The decreasing trend of σ_θ is not particularly apparent, which is because the material particles at the cavity wall yield immediately once the cavity begins to expand. When $a/a_0 > 2$, the three normal stresses increase slowly and all reach their maximum values at approximately $a/a_0 = 6$, after which the normal stresses remain constant. The maximum values of the three normal stresses increase with θ in the range of 0° – 90°. The shear stress at the cavity wall is zero when $\theta = 0°$ or 90°. This is because the cylindrical cavity must remain a circle throughout the entire expansion process. However, when $\theta = 45°$, the shear stress at the cavity wall is not always zero, $\tau_{r\theta}$ increases significantly during earlier cavity expansion stages, and when $a/a_0 > 2$, $\tau_{r\theta}$ increases slowly and all of the stresses reach their maximum values at $a/a_0 = 6$.

Fig. 7(b) presents the stress variations in material particles at r/a =5, which undergoes an elastic-to-plastic transition as the cylindrical cavity expands. The radial, vertical, and circumferential stresses change significantly during the earlier stages of the cylindrical cavity expansion. More specifically, σ_r increases while σ_z and σ_θ decrease. Before the material particles enter the plastic state, the shear stress is equal to the initial value and remains constant. After the soil yields, the shear stress decreases to a particular value owing to cavity expansion in the case of $\theta = 45°$, which indicates that the shear stress in the material particles decreases with the cavity expansion. The stress variation decreases with increasing θ compared with the case of $r/a = 1$.

Fig. 7(c) illustrates the variation of stress components in the material particles at r/a =10 where the particles are always in the elastic state (assuming that the $a/a_0 < 10$). The stress variations caused by the cavity expansion are relatively small and the shear and vertical stresses are consistently equal to their initial values. The variation trends of the radial and circumferential stresses are similar to those in the case of $r/a = 5$. With increasing θ, the stress variational ange is smaller than that in the case of $r/a = 5$. The stresses (except for the shear stress) at the cavity wall and the radius of the plastic region increase with increasing θ.

7.3 Effects of biaxial in-situ stress ratio on elastic-plastic radius

To explore the effect of the biaxial stress ratio, σ_{y0} / σ_{x0}, on the elastic-plastic radius, three sets of σ_{x0} and σ_{y0} are adopted with σ_{y0} / σ_{x0} of 2.0 and 1.6 (Cases A and C in Table 1, respectively), and three typical normalized cavity radii, a/a_0. normalized elastic-plastic radius, r_p/a. Fig. 8 shows that the elastic-plastic radius increases with increasing in-situ stress ratio. Moreover, the elastic-plastic radii with different biaxial in-situ stress ratios increase significantly with smaller a/a_0. However, when $a/a_0 > 6$, the elastic-plastic radius remains nearly constant.

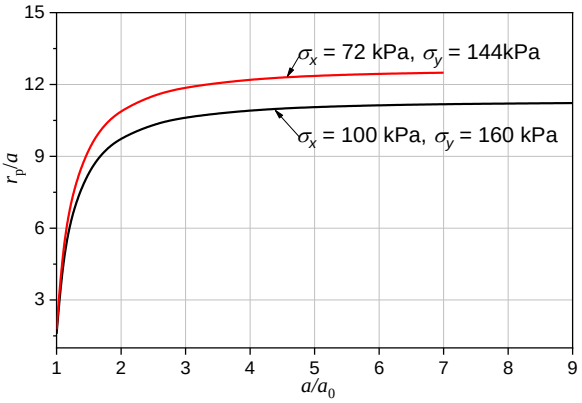

Fig. 8 Normalized elastic-plastic radius with different biaxial stress ratios obtained from the present solution

7.4 Influence of biaxial in-situ stress ratio on the E-P boundary shape

To explore the influences of σ_{x0} and σ_{y0} on the shape of the E-P boundary, three sets of σ_{x0} and σ_{y0} are adopted with σ_{y0} / σ_{x0} of 2, 1.6, and 1 (Cases A, B, and C in Table 1, respectively). Three typical a/a_0 of 1.5, 3, and 6 were adopted to represent different expansion degrees of the cylindrical cavity. Fig. 9 shows the shape variations of the E-P boundary with different biaxial stresses. When the cylindrical cavity expands under the biaxial stresses, the E-P boundary is a circle, which is inconsistent with the solution from Yang et al. (2020). The circular elastic-plastic boundaries also expand with increasing a/a_0. Moreover, the effect of σ_{y0} / σ_{x0} on the E-P boundary shape is negligible. The above phenomenon is attributed to the fact that the solution in this paper adopted the K_0-AMCC model.

From Eq. (12) the radial displacement at the E-P boundary can be expressed as

$$u_r\Big|_{r_p} = r_p - r_0 = \frac{\delta\sigma_a}{2G_0} r^p \tag{60}$$

And rearranging Eq. (60) gives

$$r_p = \frac{r_0}{1 - \dfrac{\delta\sigma_a}{2G_0}} \tag{61}$$

According to Eqs. (57) and (61), it can be concluded that the r_p is only related to p_0, OCR, G_0 and M^*, while r_p is independent of radial directions (θ). In other words, when p_0, OCR, G_0 and M^* are constant, and r_p= constant. In conclusion, it can be proved that the E-P boundary is a circle.

8. Conclusions

In this paper, a drained solution was developed based on the K_0-AMCC model for the cylindrical cavity expansion in

anisotropic soils under biaxial in-situ stresses. The solution was validated through comparisons with an existing solution.

The conclusions are summarized as follows.

- The shear stress is equal to zero at the two particular symmetric radial directions (i.e., $\theta = 0°$ and $\theta = 90°$) during the entire expansion process. The stresses (except for the shear stress) at the cavity wall and radius of the plastic region increase with increasing radial direction θ.
- The elastic-plastic radius increases with increasing the biaxial in-situ stress ratio. Moreover, the elastic-plastic (E-P) radii with different biaxial in-situ stress ratios increase significantly at a smaller normalized cavity radius.
- The elastic-plastic boundary of the cylindrical cavity expansion in the K_0-consolidated anisotropic soil under biaxial in-situ stresses is a circle rather than an ellipse in isotropic MCC soils.

Acknowledgments

This study is financially supported by the National Natural Science Foundation of China (Grant No. 41602295), the Foundation for University Key Teacher by the Ministry ofEducation of Henan Province (Grant No. 2020GGJS-094), and the Key Scientific Research Projects of Colleges and Universities in Henan Province (Grant No. 21A410002).

References

Cao, L.F., The, C.I. and Chang M.F. (2002), "Analysis of undrained cavity expansion in elasto-plastic soils with non-linear elasticity", *Int. J. Numer. Anal. Method. Geomech*., **26**(1), 25-52. https://doi.org/10.1002/nag.189.

Carter, J.P., Booker, J.R. and Yeung, S.K. (1986), "Cavity expansion in cohesive frictional soils", *Géotechnique*, **36**(3), 349-358. https://doi.org/10.1680/geot.1986.36.3.349.

Collins, I.F. and Yu, H.S. (1996), "Undrained cavity expansion in critical state soils", *Int. J. Numer. Anal. Method. Geomech*., **20**(7), 489-516. https://doi.org/10.1002/(SICI)1096-9853(199607)20:7<489::AID-NAG829>3.0.CO;2-V.

Chang, M.F., Teh, C.I. and and Cao, L.F. (2001), "Undrained cavity expansion in modified Cam clay II: Application to the interpretation of the piezocone test", *Géotechnique*, **51**(4), 335-350. https://doi.org/10.1680/geot.2001.51.4.335.

Chen, H.H., Feng, C., Li, J.P. and Sun, D.A. (2021), "Analysis of cylindrical cavity expansion in anisotropic overconsolidated clays using the Extended UH model", *Comput. Geotechnics*, **134**(3), 104-114. https://doi.org/10.1016/j.compgeo.2021.104114.

Chen, S.L. and Abousleiman, Y.N. (2013), "Exact drained solution for cylindrical cavity expansion in modified Cam Clay soil", *Géotechnique*, **63**(6), 510-517. https://doi.org/10.1680/geot.11.P.088.

Gong, W., Li, J., Li, L. and Zhang, S. (2017), "Evolution of mechanical properties of soils subsequent to a pile jacked in natural saturated clays", *Ocean Eng*., **136**, 209-217. https://doi.org/10.1016/j.oceaneng.2017.03.020.

Lamé, G. (1852), Leçons sur la théorie mathématique de l'élasticité des corps solides. Bachelier, Paris. (in French)

Li, Chao., Zou J.F. and A S.G. (2019), "Closed-form solution for undrained cavity expansion in anisotropic soil mass based on spatially mobilized plane failure criterion", *Int. J. Geomech.*, **19**(7), 04019075. https://doi.org/10.1061/(ASCE)GM.1943-5622.0001458.

Li, L., Xiang, Z.C., Zou, J.F. and Wang, F. (2019), "An improved model of compaction grouting considering three- dimensional shearing failure and its engineering application", *Geomech. Eng*., **19**(3), 217-227. https:/doi.org/10.12989/gae.2019.19.3.217.

Li, L., Gong, W. and Li, J. (2020), "Effects of clay creep on long-term load carrying behaviours of bored piles: aiming at reusing existing bored piles", *Int. J. Geomech*., **20**(8), 04020132. https://doi.org/10.1061/(ASCE)GM.1943-5622.0001769.

Liu, K. and Chen, S.L. (2019), "Analysis of cylindrical cavity expansion in anisotropic critical state soils under drained conditions", Can. Geotech. J., **56**(5), 675-686. https://doi.org/10.1139/cgj-2018-0025.

Roscoe, K. and Burland, J.B. (1968), On the generalized stress-strain behaviour of wet clay. Engineering Plasticity, Cambridge University Press.

Russell, A.R. and Khalili, N. (2002), "Drained cavity expansion in sands exhibiting particle crushing", *Int. J. Numer. Anal. Method. Geomech.*, **26**(4), 323-340. https://doi.org/10.1002/nag.203.

Salgado, R. and Prezzi M. (2007), "Computation of cavity expansion pressure and penetration resistance in sands", *Int. J. Geomech*., **7**(4), 251-265. https://doi.org/10.1061/(ASCE)1532-3641(2007)7:4(251).

Sekiguchi, H. and Ohta, H. (1977), "Induced anisotropy and time dependency in clays", *Proceedings of the Specialty Session 9, 9th ICSMFE*, Tokyo. https://doi.org/10.1007/978-1-4613-4202-1_17.

Sivasithamparam, N. and Castro, J. (2020), "Undrained cylindrical cavity expansion in clays with fabric anisotropy and structure: Theoretical solution", *Comput. Geotechnics*, **120**(3), 103386. https://doi.org/10.1016/j.compgeo.2019.103386.

Sun, D.A, Matsuoka, H, Yao, Y.P. and Ishii, H. (2004), "An anisotropic hardening elastoplastic model for clays and sands and its application to FE analysis", *Comput. Geotechnics*, **31**(1), 37-46. https://doi.org/10.1016/j.compgeo.2003.11.003.

Tan, Y.Z., Xu X., Ming H.J. and Sun D.A. (2022), "Analysis of double-layered buffer in high-level waste repository", *Annal. Nuclear Energy*, **165**, 108660. https://doi.org/10.1016/j.anucene.2021.108660.

Timoshenko, S.P. and Goodier, J.N. (1970), "Theory of elasticity", McGraw-Hill, New York, USA.

Vrakas, A. and Anagnostou, G. (2015), "A simple equation for obtaining finite strain solutions from small strain analyses of tunnels with very large convergences", *Géotechnique*, **65**(11), 738-761. https://doi.org/10.1680/geot.15.P.036.

Wood, D.M. (1990), Soil behaviour and critical state soil mechanics, Cambridge University Press, Cambridge, UK.

Wang, Y., Li, L. and Li, J.P. (2021), "A similarity solution for undrained expansion of a cylindrical cavity in K_0-consolidated anisotropic soils", *Geomech. Eng*., **25**(4), 303-315. https://doi.org/10.12989/gae.2021.25.4.303.

Yang, C., Gong, W., Li, J. and Gu, X. (2020), "Drained cylindrical cavity expansion in modified Cam-clay soil under biaxial in-situ stresses", *Comput. Geotechnics*, **121**(4), 103494. https://doi.org/10.1016/j.compgeo.2020.103494.

Yu, H.S. (2000), "Cavity expansion methods in geomechanics", Kluwer Academic Publishers, Dordrecht, Netherlands. https://doi.org/10.1007/978-94-015-9596-4.

Zhuang, P.Z. and Yu, H.S. (2019), "A unified analytical solution for elastic–plastic stress analysis of a cylindrical cavity in Mohr–Coulomb materials under biaxial in situ stresses",

Géotechnique, **69**(4), 369-376. https://doi.org/10.1680/jgeot.17.p.281.
Zhou, H., Kong, G., Liu, H. and Laloui, L. (2018), "Similarity solution for cavity expansion in thermoplastic soil", *Int. J. Numer. Anal. Method. Geomech*., **42**(2), 274-294. https://doi.org/10.1002/nag.2724.
Zhou, X.Y., He, L.Q. and Sun, D.A. (2022), "Three-dimensional thermal modeling and dimensioning design in the nuclear waste repository", *Int. J. Numer. Anal. Method. Geomech*., **46**(4), 779-797.

CC

Appendix A

A, A_r, A_θ, A_z, and $A_{r\theta}$ of the plastic stress-strain matrix are presented as follows

$$A=\frac{(\lambda-\kappa)\left(M^{*2}+\eta^{*2}\right)}{(1+e_0)\,p\left(M^{2}-\eta^{2}\right)} \tag{A1}$$

$$A_r=\frac{1}{3}+\frac{\left[3(\eta_r-\eta_{r0})-\eta_{mn}(\eta_{mn}-\eta_{mn0})\right]}{\left(M^{*2}+\eta^{*2}\right)} \tag{A2}$$

$$A_\theta=\frac{1}{3}+\frac{\left[3(\eta_\theta-\eta_{\theta0})-\eta_{mn}(\eta_{mn}-\eta_{mn0})\right]}{\left(M^{*2}+\eta^{*2}\right)} \tag{A3}$$

$$A_z=\frac{1}{3}+\frac{\left[3(\eta_z-\eta_{z0})-\eta_{mn}(\eta_{mn}-\eta_{mn0})\right]}{\left(M^{*2}+\eta^{*2}\right)} \tag{A4}$$

$$A_{r\theta}=\frac{3(\eta_{r\theta}-\eta_{r\theta0})}{\left(M^{*2}+\eta^{*2}\right)} \tag{A5}$$

B and B_{ij} of the elastoplastic constitutive equation are expressed as follows

$$B=(1+\mu)\begin{bmatrix}(1-\mu)EA(A_r^2+A_\theta^2+A_z^2)+2EA\mu(A_rA_\theta+A_rA_z+A_zA_\theta)\\+(1-2\mu)(EAA_{r\theta}^2+1+\mu)\end{bmatrix} \tag{B1}$$

$$B_{11}=E\left[(1-\mu)EAA_{r\theta}^2+EA(A_\theta^2+A_z^2+2\mu A_\theta A_z)+(1-\mu^2)\right] \tag{B2}$$

$$B_{12}=B_{21}=E\begin{bmatrix}\mu EAA_{r\theta}^2+EA(\mu A_z^2-A_rA_\theta-\mu A_rA_z-\mu A_\theta A_z)\\+\mu(1+\mu)\end{bmatrix} \tag{B3}$$

$$B_{13}=B_{31}=E\begin{bmatrix}\mu AEA_{r\theta}^2+EA(\mu A_\theta^2-A_rA_z-\mu A_rA_\theta-\mu A_\theta A_z)\\+\mu(1+\mu)\end{bmatrix} \tag{B4}$$

$$B_{14}=B_{41}=-E^2AA_{r\theta}\left[(1-\mu)A_r+\mu A_\theta+\mu A_z\right] \tag{B5}$$

$$B_{22}=E\left[(1-\mu)EAA_{r\theta}^2+EA(A_r^2+A_z^2+2\mu A_rA_z)+(1-\mu^2)\right] \tag{B6}$$

$$B_{23}=B_{32}=E\begin{bmatrix}\mu EAa_{r\theta}^2+EA(\mu A_r^2-A_\theta A_z-\mu A_rA_\theta-\mu A_rA_z)\\+\mu(1+\mu)\end{bmatrix} \tag{B7}$$

$$B_{24}=B_{42}=-E^2AA_{r\theta}\left[\mu A_r+(1-\mu)A_\theta+\mu A_z\right] \tag{B8}$$

$$B_{33}=E\left[(1-\mu)EAa_{r\theta}^2+EA(a_r^2+a_\theta^2+2\mu a_ra_\theta)+1-\mu^2\right] \tag{B9}$$

$$B_{34}=B_{43}=-E^2AA_{r\theta}\left[\mu A_r+\mu A_\theta+(1-\mu)a_z\right] \tag{B10}$$

$$B_{44}=E\begin{bmatrix}(1-\mu)EA(A_r^2+A_\alpha^2+A_\beta^2)+2E\mu A(A_rA_\alpha+A_\alpha A_\beta+A_\beta A_r)\\+1-\mu-2\mu^2\end{bmatrix}$$